The curious effect of potassium fluoride on glycerol carbonate. How salts can influence the structuredness of organic solvents

Journal of Molecular Liquids xxx (2018) xxx-xxx

Contents lists available at ScienceDirect

Journal of Molecular Liquids

journal homepage: www.elsevier.com

The curious effect of potassium fluoride on glycerol carbonate. How salts can influence the structuredness of organic solvents

Filippo Sarri[a], Duccio Tatini[a], Moira Ambrosi[a], Emiliano Carretti[a], Barry W. Ninham[b], Luigi Dei[a], Pierandrea Lo Nostro[a,*]

[a] Department of Chemistry "Ugo Schiff", University of Florence, Via della Lastruccia 3, 50019 Sesto Fiorentino(Firenze), , Italy
[b] Department of Applied Mathematics, Research School of Physical Sciences and Engineering, Australian National University, Canberra, ACT 0200, Australia

ARTICLE INFO

Article history:
Received 7 December 2017
Received in revised form 23 January 2018
Accepted 25 January 2018
Available online xxx

Keywords:
Glassy liquid
Structuredness
Ion pairs
Glycerol carbonate
Potassium fluoride

ABSTRACT

Glycerol carbonate (4-hydroxymethyl-1,3-dioxolan-2-one, shortly GC) is a dense, viscous, water soluble solvent. The high dielectric constant and dipole moment make it a suitable non-aqueous green solvent for several salts in different applications. GC dissolves significant amounts of inorganic salts such as KF. The saturation of GC with KF leads to the formation of a viscous liquid at room temperature. In this paper, we report on conductivity, rheology, differential scanning calorimetry and infrared spectroscopy experiments that indicate the formation of a glassy liquid where GC molecules and KF ion pairs are intercalated in a firm and ordered bidimensional structure, stabilized by hydrogen bonding and strong ion-dipole interactions.

1. Introduction

Cyclic carbonates, such as glycerol carbonate (GC), propylene carbonate (PC) and ethylene carbonate (EC) are associated liquids with strong intermolecular interactions, as suggested by their structural features (see Scheme 1), the large value of the Trouton constants $\Delta_{vap}S/R$ and the Kirkwood parameter g (see Table 1) [1,2].

These liquids find remarkable applications in several industrial fields [3,4]. In particular they are excellent solvents for electrolytes, due to their very high dielectric constant and dipole moment that determine the dissociation of ions and promote ion-solvent interactions, respectively. Moreover, in the case of GC a terminal primary –OH residue further increases the structuredness of the solvent and can assist in the ion solvation through hydrogen bonding (HB). In glass-forming liquids molecules are disordered though strongly interacting. PC and glycerol are examples of low-molecular-weight organic glass formers [5].

Molecular liquids like GC, usually show an excellent glass-forming ability, which is related to the strength of the intermolecular interactions (van der Waals forces and hydrogen bonds) [6,7]. These materials exhibit distinctly non-liquid-like features, a soft glassy rheology, which make them very attractive for technological applications and intriguing systems in terms of physics of condensed matter [8,9]. Indeed, several technical applications take advantage of GC physico-chemical properties. These include the technology of lithium and lithium-ion batteries, cement and concrete industries, sugar cane treatment, cosmetics and detergents [1,10–12].

In spite of the increasing interest in innovative synthetic routes for the production of GC [13,14], aimed at reducing the costs and enhancing the yield, only few articles on the GC physico-chemical properties have appeared in the literature.

While studying the solubility of some electrolytes in different cyclic carbonates in terms of the Hofmeister series [1], we came across a peculiar behavior of saturated solutions of KF in GC. In this paper we report our results from conductivity, viscosity, calorimetric and infrared measurements that reflect the formation of a dense and viscous glassy liquid at room temperature.

2. Experimental

2.1. Materials

Glycerol carbonate and potassium fluoride (99%) were purchased from Sigma-Aldrich (Milan, Italy). The salt was purified, dried and stored under vacuum, according to the standard procedures [1a,b]. Glycerol carbonate was used as received and kept under inert atmosphere to avoid water contamination.

2.2. Electric conductivity measurements

A Metrohm 712 conductimeter with a 0.83 cm^{-1} cell constant was used. Salt concentrations ranged between 0 and 1.5 M. The cell was immersed in a thermostatted water bath to control the temperature of the sample (25.0 ± 0.1 °C).

* Corresponding author.
Email address: pierandrea.lonostro@unifi.it (P.L. Nostro)

https://doi.org/10.1016/j.molliq.2018.01.152
0167-7322/

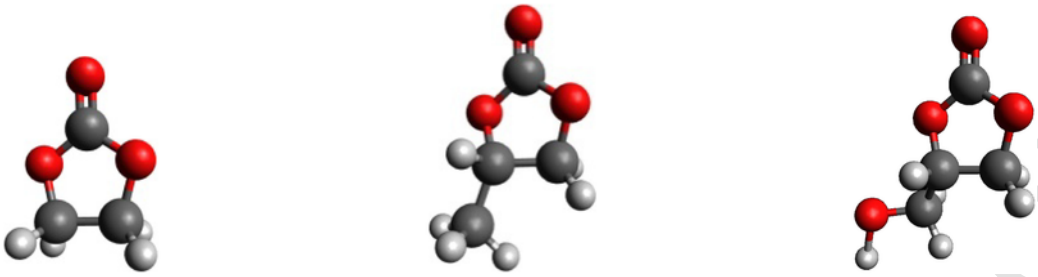

Scheme 1. From left to right: minimized chemical structures of EC, PC and GC. Grey, red and white spheres represent carbon, oxygen and hydrogen atoms, respectively.

Table 1
Physico-chemical properties of glycerol, propylene and ethylene carbonate at 25 °C.

Property	GC	PC	EC[a]
Dielectric constant, ε	109.7	64.9	89.8
Dipole moment, μ (D)[b]	5.05	5.36	4.81
Viscosity, η (cP)	85.4[c]	2.53	1.90
Density, ρ (g/mL)	1.3969[d]	1.200	1.321
Trouton constant, $\Delta_{vap}S/R$	34.6	11.6	12.1
Kirkwood parameter, g	8.18	1.23	1.60

[a] At 40 °C.

[b] From Ref. [4].

[c] From Ref. [3].

[d] This work.

2.3. Rheology measurements

Rheology measurements were acquired with a Paar Physica UDS 200 rheometer working in the controlled shear-stress mode. For all samples a plate–plate geometry (diameter, 4 cm; gap, 300 μm) was used. All measurements were performed at (25.00 ± 0.01) °C. For each sample the flow curve was acquired in a torque range from 10^{-3} to 2000 mNm. The sample equilibrated for 15 min at the set temperature before running the measurement.

2.4. Differential scanning calorimetry

Differential Scanning Calorimetry (DSC) runs were carried out on a DSC-Q2000 from TA Instruments (Milan, Italy). The samples were first equilibrated at −30 °C, then cooled from −30 °C to −90 °C at 2 °C/min, and finally heated up to −30 °C at 2 °C/min. The experiments were conducted under N_2 atmosphere with a flow rate of 50 mL/min. The thermograms were analyzed by the TA Universal Analysis software. For all samples the glass transition temperatures (T_g) were obtained from the inflection point in the DSC signal.

2.5. Attenuated total reflection Fourier-transform infrared spectroscopy

Attenuated total reflection Fourier-transform infrared spectroscopy (ATR-FTIR) spectra were acquired using a Thermo Nicolet Nexus 870 FT-IR spectrophotometer, equipped with a liquid nitrogen cooled MCT (mercury-cadmium-telluride) detector, by averaging on 128 scans at a resolution of 2 cm^{-1} and with CO_2-atmospheric correction. The spectra were acquired in the range 4000–900 cm^{-1}. For each spectrum the background was previously recorded and subtracted to the sample profile.

3. Results and discussion

3.1. Electric conductivity measurements

The conductivity of KF + GC samples was measured at 25.0 °C as a function of the salt concentration (c). Fig. 1 shows the specific conductivity κ and the molar conductivity Λ of KF + GC solutions as a function of c. The data of κ and Λ were fitted according to the Casteel-Amis equation [15], and to the Fuoss-Kraus model, respectively (see Appendix A) [16].

In the dilute regime κ raises with c due to the increasing number of charge carriers. At moderate-to-high concentrations ($c > 1$ M), as

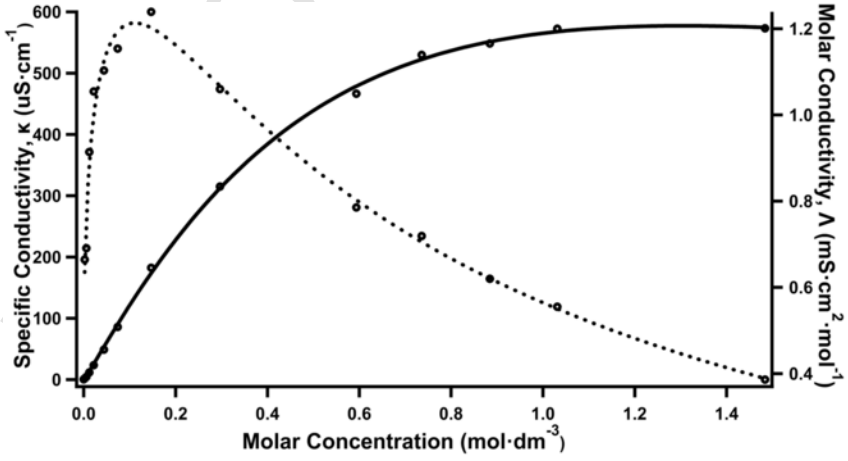

Fig. 1. Specific conductivity κ (solid line) and molar conductivity Λ (dashed line) for KF solutions in GC as a function of the molar concentration of the salt (c). The lines serve as a guide to the eyes.

the ion-ion interactions strengthen and the viscosity of the medium increases, the curve shows a plateau due to the competition between the increase in the number of charge carriers and the decrease in ionic mobilities [17]. For $c > 1.5$ M the solution becomes turbid presumably due to the formation of larger particles and we observed the onset of an intense yellowing, that preludes to the degradation of GC [18].

The Casteel-Amis model fits the experimental data with good agreement. The trend recorded for κ confirms that at moderate-to-high concentrations stronger ion-ion interactions come into play and rule over other forces in setting the ionic conductivity [19].

The plot of Λ vs. c (Fig. 1) provides interesting insights into the solvent-solute interactions. The curve shows a rapid increase in the dilute regime, then reaches a maximum at about 0.15 M and progressively decreases when c further increases. The presence of a maximum is a typical behavior that suggests the formation of ion pairs and triple ions (K_2F^+ and KF_2^-) [20]. In most cases the maximum is preceded by a minimum, corresponding to the onset of triple ions formation [12]. In our system this minimum is not observed, indicating that the ion association is predominant and the formation of charged triplets already occurs at very low c values. The Λ data were analyzed in terms of the Fuoss-Kraus model (see Fig. A1 in Appendix A) from which the association constants for ion pairs (K_I) and for triple ions (K_T) can be estimated (see Appendix A) [16,21].

K_I is about $2.8 \cdot 10^6$, confirming the high tendency for K^+ and F^- to form ion pairs, while K_T is about 550, that reflects the formation of triple ions in GC. While the formation of ion pairs is typical for solutions of salts in polar organic solvents, the creation of triple ions at the extent recorded here was unexpected. From these values the fraction of triplets, ion pairs and free ions (α_T, α_P, and α_I, respectively) can be calculated as described in Appendix A [16,21].

The distribution curves for α_T, α_P, and α_I are reported in Fig. 2. KF ion pairs are always the most abundant species ($\alpha_P > 0.8$), with a very small fraction of free ions ($\alpha_I < 0.02$). The fraction of triple ions increases from 0.01 to 0.18 as more KF is added.

These findings lead to two important conclusions: (i) The lack of a minimum in the Λ/c plot is due to the high concentration of the non-conductive ion pairs even at very low contents of KF, and to the decrease in their fraction as triple ions are formed. Thus, the major contribution to the conductivity is provided by the triple ions, and this results in the maximum in the Λ/c curve. (ii) These data suggest that GC, despite its remarkably high dielectric constant, does not effectively solvate and separate K^+ and F^-, that rather remain associated in ion pairs (or triplets, at higher c). This can be explained in terms of the strong intermolecular interactions, on the structuredness of the pure liquid, and on the asymmetry between the interactions of the terminal –OH moiety with anions and the carbonyl oxygen with cations in GC.

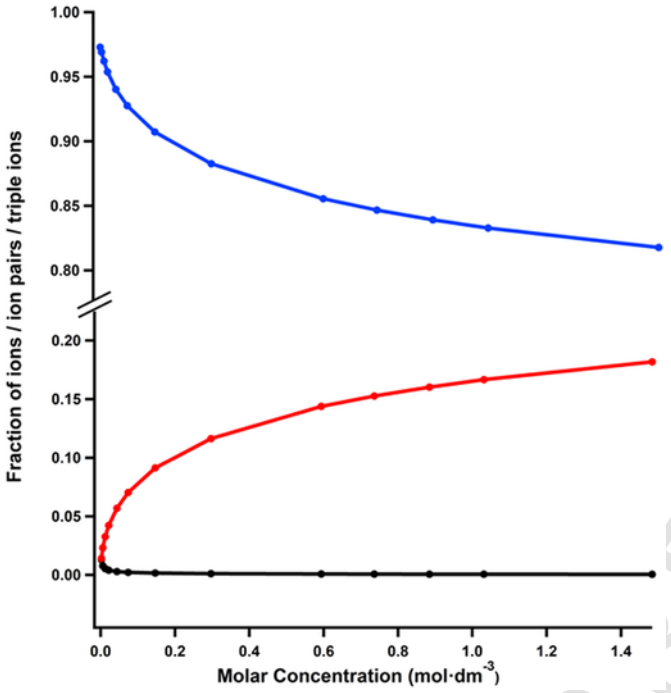

Fig. 2. Calculated fractions for triple ions (red), ion pairs (blue) and free ions (black) for KF in GC at 25 °C. (For interpretation of the references to colour in this figure legend, the reader is referred to the web version of this article.)

3.2. Rheology measurements

Rheology measurements were performed at 25.0 °C. The flow curve for pure GC (see Fig. A2 in Appendix B) shows a remarkable hysteresis in the viscosity data of the pure liquid when an increasing stress is first applied and then reduced. To the best of our knowledge this is the first report on the thixotropic nature of GC due to its intrinsic structuredness. Fig. 3 reports the flow curves for pure GC and with increasing concentrations of KF between 10^{-3} M and 0.68 M.

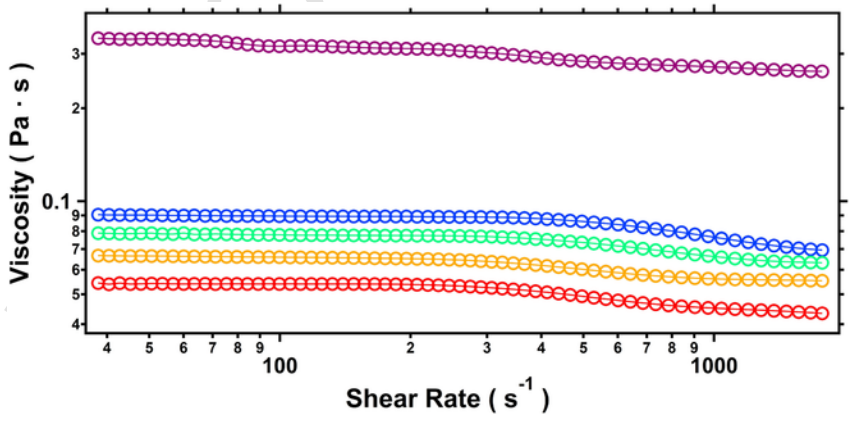

Fig. 3. Flow curves acquired on pure GC (red) and on KF + GC solutions at different salt concentrations: $7 \cdot 10^{-3}$ M (yellow), $7 \cdot 10^{-2}$ M (light blue), 0.21 M (blue), and 0.68 M (purple). (For interpretation of the references to colour in this figure legend, the reader is referred to the web version of this article.)

The viscosity of KF + GC solutions increases as a function of the solute concentration. However, when the KF content is further increased, the viscosity steeply grows and exceeds by >10 times the value found for the pure solvent. This suggests that KF induces a very significant change in the solvent ordering, by forcing the formation of a stronger and more viscous structure in the medium.

The fractions of triple ions, ion pairs and free ions obtained from the conductivity data were used in a modified Jones-Dole equation (Eq. (1)), that describes the variation of the solution viscosity η as a function of the solute concentration c [22], by including two terms that take into account the effect of free ion-solvent and ion pair-solvent interactions [23,24]:

$$\eta = \eta_0 \left[1 + A \sqrt{(\alpha_i + \alpha_t)\ c} + \mathrm{B}_i\ (\alpha_i + \alpha_t)\ c + B_p\ \alpha_p\ c + \boldsymbol{D}\ c^2 \right] \quad (1)$$

here η_0 is the viscosity of the pure solvent at the same temperature, A is the Falkenhagen coefficient that takes into account the electrostatic forces [25], B_i and B_p are the Jones-Dole coefficients that account for the ion-solvent and the ion pair-solvent interactions, respectively, and D is an additional term related to higher order solute-solute interactions. This equation is specifically targeted to fit cases where the salt concentration is relatively high, $c \geq 0.1$ M, and ion pair association is non negligible [23], whereas when $c < 0.1$ M the higher order term Dc^2 is usually overlooked [26–30].

η was recorded at an applied stress of 10 Pa and plotted versus c (see Fig. A3 in Appendix C). The values of A, B_i, B_p and D were calculated by fitting the experimental data according to Eq. (1). We obtained positive values for A and B_p (0.11 $dm^{3/2}\,mol^{-3/2}$ and 4.22 $dm^3\,mol^{-1}$, respectively); whereas, both B_i and D are negative (−0.92 $dm^3\,mol^{-1}$ and −7.67 $dm^6\,mol^{-2}$, respectively). This result and the rise in the viscosity suggest that ion pairs are the most represented species in solution. We recall that the Jones-Dole B coefficient is positive for cosmotropes and negative for chaotropes, e.g., B is 0.127 for F^-, and −0.009 $dm^3\,mol^{-1}$ for K^+ (in water, at 25 °C) [31]. Interestingly we note that in the present case B_i, which is due to the free ionic species (mainly K^+, F^-, K_2F^+ and KF_2^-) that singularly destroy the structure of liquid GC, is large and negative. Instead, B_P is positive, suggesting that the ion pairs enhance the order of the solvent molecules.

3.3. Differential scanning calorimetry

The thermal behavior of pure GC and of its KF saturated solution was investigated through Differential Scanning Calorimetry (DSC). The DSC scans are reported in Fig. 4. Glycerol carbonate has a remarkably large range of stability with a high boiling point and a very low melting temperature [3]. From the DSC experiments we detected a glass transition temperature (T_g) at −70.8 °C for the pure GC and at −61.3 °C for the KF saturated solution. A similar behavior was reported for glycerol and PC [32,33]. The heat flow signal suggests the presence of an enthalpic recovery associated to the glass transition. The two contributions, namely the ΔC_p at the glass transition temperature (T_g), and the endothermic peak due to the enthalpic recovery process, cannot be separated by standard DSC. The remarkable increment in the T_g of the liquid upon the addition of KF confirms a strong stiffening effect induced by the electrolyte on the solvent molecules structuredness.

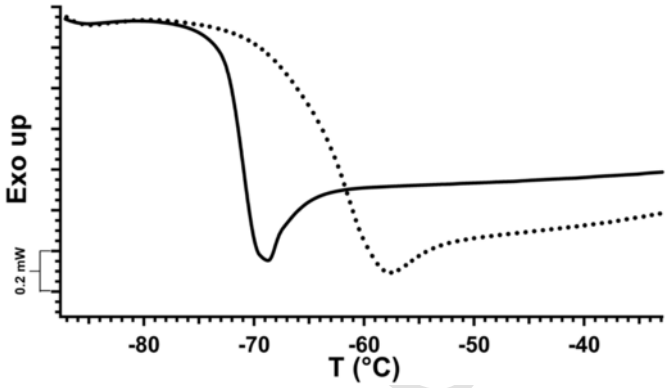

Fig. 4. DSC runs for pure GC (solid line) and for the KF saturated solution (dotted line).

3.4. Attenuated Total reflection-Fourier transform infrared spectroscopy

The Attenuated Total Reflection-Fourier Transform Infrared Spectroscopy (ATR-FTIR) experiments (see Fig. 5) indicate that an increment in the KF concentration brings about a shift in the O—H stretching band from 3420 cm^{-1} for pure GC, to 3370 cm^{-1} for the 0.68 M KF sample. Most likely this finding reflects the interaction between the hydroxyl moiety and the fluoride anion, that leads to a weakening in the O—H stretching mode. Further addition of KF results in a more significant shift of the band to lower wavenumbers.

Importantly, the addition of KF does not modify the FTIR profile of pure glycerol carbonate (see Fig. A4 in Appendix D). In fact the position of the absorption bands of GC is not affected by the addition of the salt [34,35]. In particular, the CH_2 and CH vibrations of the cyclic carbons remain unaffected (2990–2880 cm^{-1}). The C═O stretching is slightly shifted to lower wavenumbers (from 1791 cm^{-1} for the pure liquid to 1766 cm^{-1} for 0.68 M solution) probably due to the interaction of the carbonyl moiety with the potassium cation. The C—C and C—O stretching of the 2-hydroxyethyl chain appear at 1167 and 1047 cm^{-1} and are not modified by the addition of KF.

The O—H stretching peak decreases as a function of the KF concentration (Fig. 6) due to the stronger solvent-salt interactions while more salt is added.

A lighter and opposite effect was found in the case of the C═O stretching, whose wavenumber increases at high concentrations of KF, as indicated by Fig. 7. We argue that when the concentration of potassium fluoride is large the pristine HB between the carbonyl residue and the primary –OH group is remarkably weakened, as F^- substitutes the carbonyl's O. At the same time the purely electrostatic (ion-dipole) interaction between K^+ and the carbonyl of the GC molecule is weaker than the C═O···H—O hydrogen bonding, resulting in a shift in the infrared peak for the C═O stretching mode. Thus, the basic nature of the fluoride ion seems to be the main driving force that modifies the structuredness of the solvent molecules in ordered domains.

4. Conclusion

In conclusion the experimental results apparently suggest a remarkable strenghtening in the structuredness of liquid glycerol carbonate upon addition of potassium fluoride.

Literature sources on the behavior of fluoride ions in non-aqueous solvents report that F^- is scarcely solvated in aprotic solvents, with a

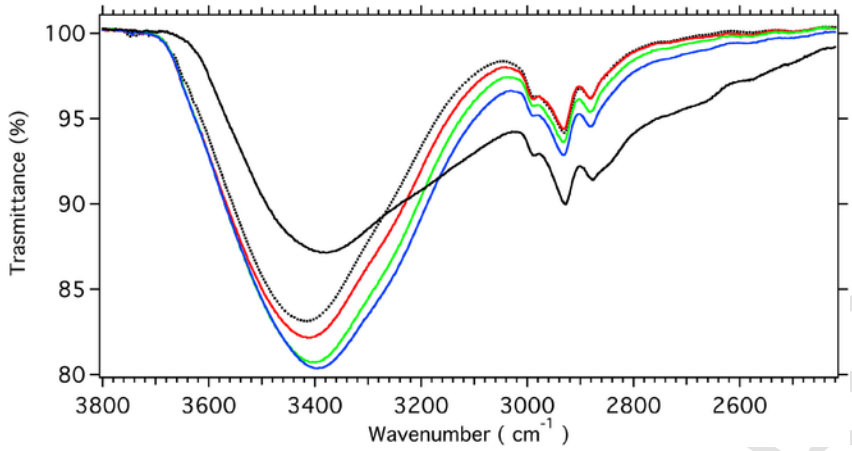

Fig. 5. Attenuated Total Reflection-Fourier Transform Infrared (ATR-FTIR) spectra between 3800 and 2400 cm^{-1} for pure GC (dotted line) and GC+KF solutions at different salt concentration: $7{\cdot}10^{-3}$ M (red), $7{\cdot}10^{-2}$ M (green), 0.21 M (blue), and 0.68 M (black). The whole spectra are shown in Fig. A4 in Appendix D. (For interpretation of the references to colour in this figure legend, the reader is referred to the web version of this article.)

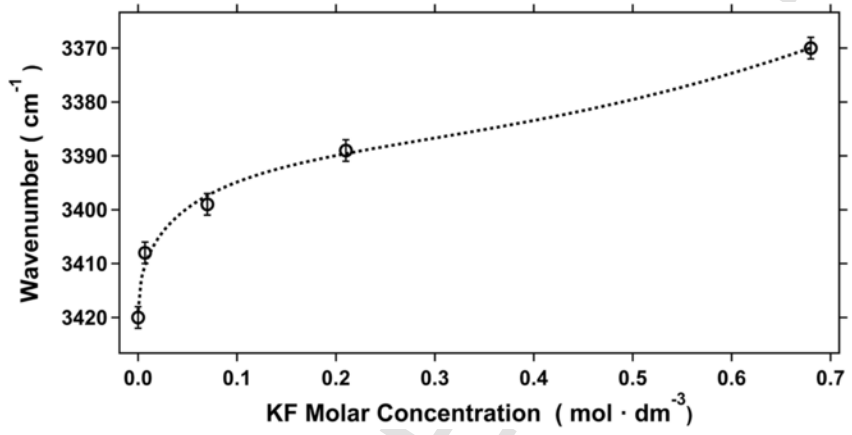

Fig. 6. Shift of the ATR—IR O—H stretching band wavenumber versus the KF concentration. The dotted black line is a guide for the eye.

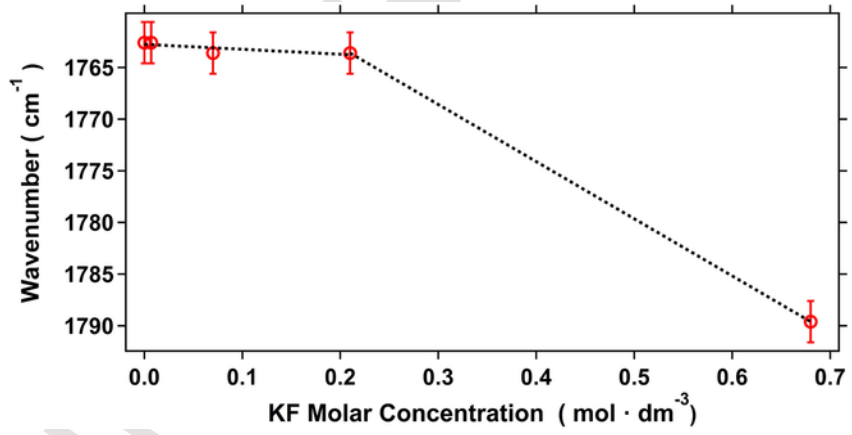

Fig. 7. Shift of the ATR—IR C═O stretching band wavenumber versus the KF concentration. The dotted black line is a guide for the eye.

lower basicity and a higher nucleophilicity. On the other hand, in protic solvents F^- greatly interacts with the solvent molecules through HB, leading to a higher basicity [45,46].

The cartoon in Fig. 8 schematically depicts a hypothetical structure of the solution where the solvent molecules (green arrows) are organized in wormlike structures intercalated by KF ion pairs with which they interact through ion-dipole interactions (between K^+ and the C═O residue) and HB between F^- and the –OH moiety of GC. The dissolved KF salt mainly forms ion pairs that are responsible for the remarkable increase in the viscosity of the solution. A similar or-

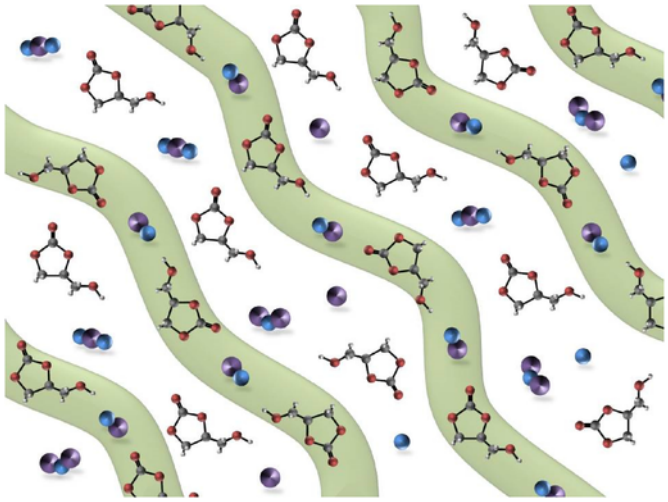

Fig. 8. Schematic cartoon showing the proposed structure that comprises ordered domains of GC molecules with a head-to-tail orientation intercalated by KF ion pairs. In the opposite direction the GC dipoles are inverted. The large purple and the light blue globes represent potassium and fluoride ions, respectively. K^+, F^- and triple ions are dispersed in the solution.

dering was proposed by Jones for the dissolution of LiF in EC or PC [2]. Free solvated K^+ and F^- and triple ions are present and contribute to the overall conductivity of the sample.

In the side directions, along the main axis the solvent molecules are oriented in the opposite way, as required by the minimization of the dipoles energy. Such ordered structure would justify the conductivity and viscosity features of this glassy liquid system. Further structural investigations through SAXS and NMR experiments and solubility assessments are currently in progress.

Appendix A. Casteel-Amis Equation and Fuoss-Kraus Formalism

The specific conductivity (κ) was fitted according to the Casteel-Amis model that provides an empirical equation commonly used to describe the conductivity behavior of electrolytes over wide ranges of salt concentration [15,36]. In this model the relation between κ and the concentration m (in molal units) is expressed as:

$$\frac{\kappa}{\kappa_{\max}} = \left(\frac{m}{\mu}\right)^a \exp\left[b(m-\mu)^2 - \frac{a}{\mu}(m-\mu)\right] \tag{A1}$$

where $\kappa_{\max}$ is the maximum value of conductivity, μ is the concentration at which $\kappa_{\max}$ is reached, and a and b are fitting parameters (see Table A1). $\kappa_{\max}$ and μ are mainly determined by the solvent viscosity and the ionic radii [37].

Table A1 The parameters a, b, μ and $\kappa_{\max}$ obtained by fitting the specific conductivity data with the Casteel-Amis equation.

μ	κ_{max}	a	b	χ^2
0.89±0.06	577±4	1.08±0.05	0.316±0.141	375

More recent approaches describe the conductivity of strong electrolyte solutions at moderate-to-high concentrations in polar non-aqueous solvents. The "quasi-lattice theory" or the mean spherical approximation (MSA) method are some examples [17 and references therein]. These models do not fit accurately our data, thus we decided to use a modified semi-empirical version of the Fuoss-Kraus model, which provides a quantitative estimation of the ionic fractions in solution from conductivity measurements [16]. This model is widely used for polyelectrolytes-based systems [38–40]. The method requires the determination of the limiting conductivities, then the calculation of ion pair and triplets conditional formation constants and finally the fractions of triplets, ion pairs and "free" ions as a function of the salt concentration [41].

Assuming that only KF, K^+, F^-, K_2F^+ and K_2F^- are present in the solution (i.e. no quadrupoles or higher charged clusters), the KF ion pair can either dissociate in free ions:

$$KF \rightarrow K^+ + F^-$$

or triplets:

$$3\,KF \rightarrow KF_2^- + \ K_2F^+$$

From the calculation of the activity coefficients through the extended Debye-Hückel theory and the Bjerrum formula [1a,b] we found that $\gamma_\pm$ ranges between 0.94 and 0.96, thus we used the approximation of unitary coefficients. Moreover, assuming that the concentrations of K_2F^+ and K_2F^- are equal, the corresponding conditional association constants K_I and K_T for ion pairs and triplets are related to the ion fractions in the following manner:

$$K_I = \frac{[KF]}{[K^+][F^-]} = \frac{1-\alpha_I}{{\alpha_I}^2} \tag{A2}$$

$$K_T = \frac{\left[KF_2^-\right]}{[KF][F^-]} = \frac{\left[K_2F^+\right]}{[KF][K^+]} = \frac{\alpha_T}{\alpha_I c\left(1-\alpha_I-3\alpha_T\right)} \tag{A3}$$

where α_I and α_T are the free ions and triplets fractions respectively. From which we obtain:

$$\alpha_I = \frac{-1+\sqrt{1+4K_Ic}}{2K_Ic} \tag{A4}$$

$$\alpha_T = \frac{K_T\alpha_I\left(1-\alpha_I\right)c}{1+3K_T\alpha_Ic} \tag{A5}$$

$$\alpha_P = 1-\alpha_I-\alpha_T \tag{A6}$$

$\alpha_P$is the fraction of ion pairs. If we do not consider the effect of the electrostatic field generated by the ions, the total molar conductivity is expressed as:

$$\Lambda = \alpha_I {\Lambda_0}^I + \alpha_T {\Lambda_0}^T \tag{A7}$$

where ${\Lambda_0}^I$ and ${\Lambda_0}^T$ are the limiting molar conductivities in GC for the free ions and the triple ions respectively. Thus, replacing the expressions for α_I and α_T and rearranging the equation, we obtain:

$$\Lambda\sqrt{c} = \frac{{\Lambda_0}^I}{\sqrt{K_I}} + \frac{{\Lambda_0}^T K_T c}{\sqrt{K_I}} \tag{A8}$$

In the dilute regime, the plot of $\Lambda\sqrt{c}$ vs. c produces a linear relation with a slope of ${\Lambda_0}^T K_T {K_I}^{-1/2}$ and an intercept of ${\Lambda_0}^I {K_I}^{-1/2}$. In order to calculate the values of K_I and K_T, ${\Lambda_0}^I$ and ${\Lambda_0}^T$must be determined. We assume that ${\Lambda_0}^I = \Lambda_0$, since at infinite dilution ion-ion interactions vanish and triple ions formation can be neglected. The value of Λ_0 from the limiting molar conductivities (λ_i) can be estimated as:

$$\Lambda_0 = \sum_i \nu_i \lambda_i \tag{A9}$$

where ν_i is the number of i ions in the formula unit of the electrolyte.

The limiting molar conductivity λ_i is related to the ionic mobility u_i according to [42]:

$$\lambda_i = z_i F u_i \tag{A10}$$

where F is the Faraday constant and z_i is the charge of the i ion. The ionic mobility is defined as [43]:

$$u_i = \frac{e z_i}{6\pi\eta_0 r_{hi}} \tag{A11}$$

where e is the elementary charge, z_i is the charge of the i ion, η_0 is the solvent viscosity and r_{sol} is the solvated radius of the i ion. Assuming a spherical geometry for the solvated ion, its solvated radius can be calculated as:

$$\frac{4}{3}\pi r_{sol}^3 = \frac{4}{3}\pi r_{cryst,i}^3 + n_s \bullet V_s \tag{A12}$$

where n_s is the number of solvent molecules in the solvation layer around the ion, V_s is the molar volume of a solvent molecule and $r_{cryst,\,i}$ is the crystalline radius of the ion. We calculated the ionic mobilities and the conditional association constants K_I and K_T for n_s values ranging between 1 and 5. The value of n_s has a negligible influence on the ionic mobilities and on the conditional association constants. Moreover, considering also the effects due to the steric hindrance, we assumed an average solvation number of 3. Once Λ_0 is obtained, ${\Lambda_0}^T$ is taken as $2\Lambda_0/3$ (${\Lambda_0}^T$cannot be determined experimentally) [44].

The values of the ionic mobilities (u, in A·s^2/kg) and the limiting molar conductivities (λ and Λ, in S·m^2/mol) in GC are shown in Table A2:

Table A2 Calculated ionic mobilities (u, in A·s^2/kg) and limiting molar conductivities (λ and Λ, in S·m^2/mol) for K^+ and F^- in GC at 25 °C.

u_{K^+}	u_{F^-}	λ_{K^+}	λ_{F^-}	$\Lambda_0=\lambda_{K^+}+\lambda_{F^-}$
$4.73\cdot10^{-10}$	$4.87\cdot10^{-10}$	$4.56\cdot10^{-5}$	$4.70\cdot10^{-5}$	$9.26\cdot10^{-5}$

For the triple ions, ${\Lambda_0}^T = \frac{2}{3}\Lambda_0 = 6.17\cdot10^{-5}$ S m^2/mol.

The plot of $\Lambda\sqrt{c}$ as a function of c (see Fig. A1) shows a linear trend in the dilute regime, up to approximately 22 mM. The slope and intercept are $2.03\cdot10^{-5}\pm9\cdot10^{-7}$ S dm$^{7/2}$ mol$^{-3/2}$ and $5.54\cdot10^{-8}\pm1\cdot10^{-8}$ S m$^{1/2}$ mol$^{1/2}$ respectively.

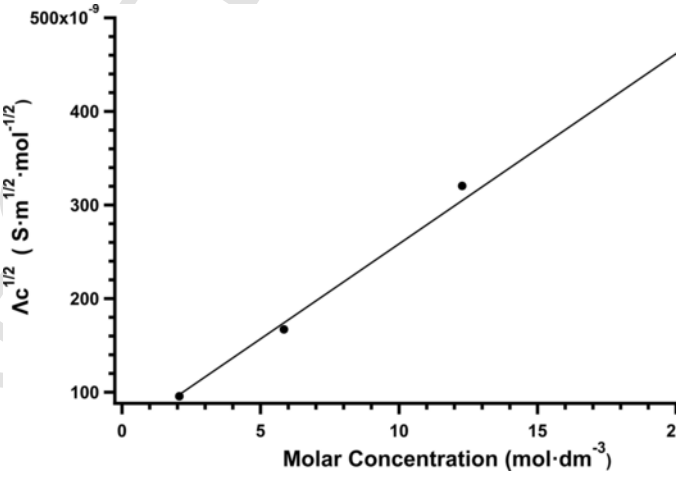

Fig. A1. Plot of $\Lambda\sqrt{c}$ as a function of c.

Eqs. (A2) and (A3) provide the values of K_I and K_T: $K_I = (2.8\pm0.4)\cdot10^6$ and $K_T = 550\pm235$, from which the values of α_I, α_T and α_P can be calculated.

Appendix B. Thixotropy in glycerol carbonate

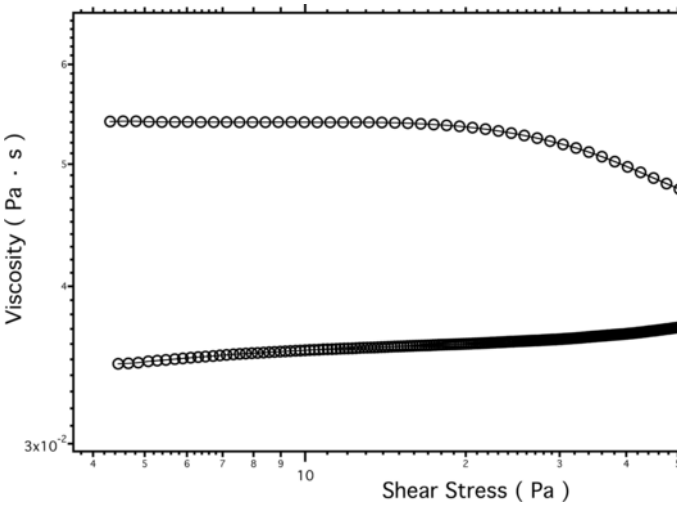

Fig. A2. Thixotropic behavior of pure GC.

Fig. A2 shows the flow curve of pure glycerol carbonate acquired in two steps: the applied stress was first increased and then restored to the initial value. The hysteresis of the curve reflects the thixotropic nature of the solvent and gives a further evidence of its structuredness.

Appendix C. Extended Form of the Jones-Dole Equation

The viscosity values at 10 Pa were plotted vs. the KF concentration and fitted with a modified Jones-Dole equation (Fig. A3). Indeed, when ionic association occurs the Jones-Dole B coefficient is split in two different contributions: the first (B_i) is related to the interactions between the solvent and the charged species, whereas the second term (B_p) takes into account the solvent-ion pairs interactions. When the salt concentration exceeds the value of 0.1 M an additional term (D) is added to take into account the solute-solute interactions of higher order [26–29]. The equation then becomes:

$$\eta = \eta_0 \left[1 + A\sqrt{(\alpha_i + \alpha_t)\,c} + B_i(\alpha_i + \alpha_t)\,c + B_p\,\alpha_p\,c + Dc^2\right] \quad \text{(A13)}$$

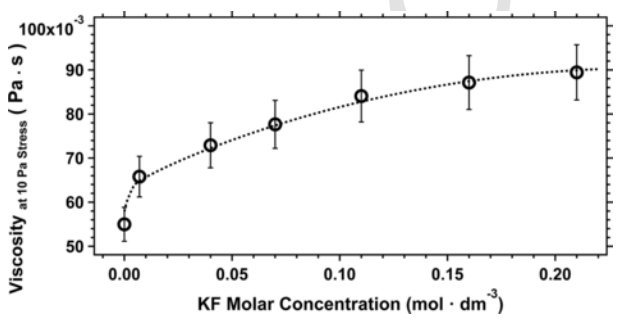

Fig. A3. Viscosity values plotted vs. the salt concentration for KF+GC solutions at 25 °C. The curve is obtained by fitting the experimental data with Eq. (A13) and the fitting parameters are listed in Table S3.

Table S3 Fitting parameters obtained from Eq. (13).

A	B_i	B_p	D	χ^2
0.11 ± 0.02	−0.92 ± 0.17	4.22 ± 0.72	−7.68 ± 0.97	$3.6\cdot10^{-3}$

Moreover, the theoretical Falkenhagen coefficient for GC was calculated as reported by Jenkins and Marcus [24], and compared to the fitting value:

$$A = \frac{A_*}{\eta_0 \bullet \sqrt{\varepsilon_r \bullet T}} \bullet f\left(\lambda_+^\infty, \lambda_-^\infty\right) \quad \text{(A14)}$$

where A_* is $1.113\cdot10^{-5}$ C (m·K·mol^{-3})$^{1/2}$, ε_r is the dielectric constant of the solvent, T is the absolute temperature, and $f(\lambda_+{}^0, \lambda_-{}^0)$ is the ions infinite dilution equivalent conductivities function that, in the case of symmetrical electrolytes ($z_+ = |z_-| = z$), is defined as:

$$f = \left[\frac{z^2\left(\lambda_+^\infty + \lambda_-^\infty\right)}{4\left(2+\sqrt{2}\right)\left(\lambda_+^\infty \bullet \lambda_-^\infty\right)}\right] \bullet \left[1 - \frac{4\left(\lambda_+^\infty - \lambda_-^\infty\right)^2}{\left(1+\sqrt{2}\right)^2\left(\lambda_+^\infty + \lambda_-^\infty\right)^2}\right] \quad \text{(A15)}$$

From Eq. (A14) the calculated value for A comes out to be 0.11 dm$^{3/2}$/mol$^{3/2}$, in very good agreement with the value obtained from the fitting procedure.

Appendix D. ATR-FTIR Results

The ATR-FTIR spectra acquired in the range 4000–900 cm^{-1} for pure GC and GC+KF solutions at different salt concentration ($7\cdot10^{-3}$ M, $7\cdot10^{-2}$ M, 0.21 M, and 0.68 M) are reported in Fig. A4.

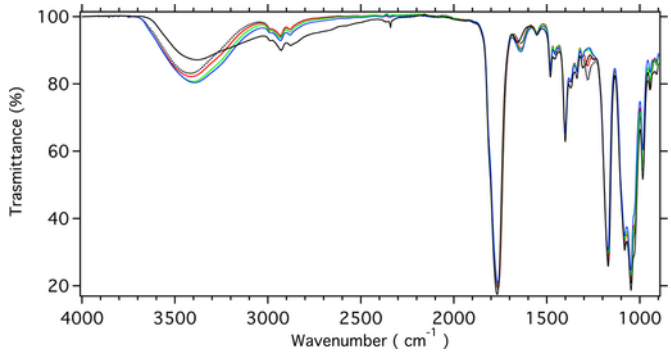

Fig. A4. ATR-FTIR spectra acquired on pure GC (black dotted line) and on KF + GC solutions at different salt concentrations: $7 \cdot 10^{-3}$ M (red), $7 \cdot 10^{-2}$ M (green), 0.21 M (blue), and 0.68 M (black solid line).

References

[1] a) N. Peruzzi, B.W. Ninham, P. Lo Nostro, P. Baglioni, J. Phys. Chem. B 116 (2012) 14398;
b) N. Peruzzi, P. Lo Nostro, B.W. Ninham, P. Baglioni, J. Solut. Chem. 44 (2015) 1224.
[2] J. Jones, M. Anouti, M. Caillon-Caravanier, P. Willmann, D. Lemordant, Fluid Phase Equilib. 285 (2009) 62.
[3] M.O. Sonnati, S. Amigoni, E.P. Taffin de Givenchy, T. Darmanin, O. Choulet, F. Guittard, Green Chem. 15 (2013) 283.
[4] Y. Chernyak, J. Chem. Eng. Data 51 (2006) 416.
[5] X.N. Ying, Phys. Scr. 88 (2013), 025603.
[6] U.R. Pedersen, P. Harrowell, J. Phys. Chem. B 115 (2011) 14205.
[7] K. Koperwas, K. Adrjanowicz, Z. Wojnarowska, A. Jedrzejowska, J. Knapik, M. Paluch, Sci. Rep. 6 (2016) 36934.
[8] R. Zondervan, T. Xia, H. van der Meer, C. Storm, F. Kulzer, W. van Saarloos, M. Orrit, PNAS 105 (2008) 4993.
[9] M. Köhler, P. Lunkenheimer, A. Loid, Eur. Phys. J. E 27 (2008) 115.
[10] Z. Zhang, D.W. Rackemann, W.O.S. Doherty, I.M. O'Hara, Biotechnol. Biofuels 6 (2013) 153.
[11] M. Pagliaro, R. Ciriminna, H. Kimura, M. Rossi, C. Della Pina, Angew. Chem. Int. Ed. 46 (2007) 4434–4440.
[12] J.R. Ochoa-Gómez, O. Gómez-Jiménez-Aberasturi, C. Ramírez-López, M. Belsué, Org. Process. Res. Dev. 16 (2012) 389.
[13] P.U. Okoye, A.Z. Abdullah, B.H. Hameed, J. Taiwan Inst. Chem. Eng. 68 (2016) 51.
[14] P.U. Okoye, A.Z. Abdullah, B.H. Hameed, Energy Convers. Manag. 133 (2017) 477–485.
[15] J.F. Casteel, E.S. Amis, J. Chem. Eng. Data 17 (1972) 55.
[16] C. Kraus, R. Fuoss, J. Am. Chem. Soc. 55 (1933) 21.
[17] K. Izutsu, Electrochemistry in Nonaqueous Solutions, Wiley-VCH, Weinheim, 2002201–222.
[18] D.J. Darensbourg, A.D. Yeung, Green Chem. 16 (2014) 247.
[19] R. Jan, G.M. Rather, M.A. Bhat, J. Solut. Chem. 43 (2014) 685.
[20] G. Macfie, M.G. Compton, H.R. Corti, J. Chem. Eng. Data 46 (2001) 1300.
[21] D. Aurbach, Nonaqueous Electrochemistry, CRC Press, 1999.
[22] G. Jones, M. Dole, J. Am. Chem. Soc. 51 (1929) 2950.
[23] A. Kacperska, S. Taniewska-Osinska, A. Bald, A. Szejgis, J. Chem. Soc., Faraday Trans. 1 85 (1989) 4147.
[24] H.D.B. Jenkins, Y. Marcus, Chem. Rev. 95 (1995) 2695.
[25] H. Falkenhagen, E.L. Vernon, Phylos. Mag. 14 (series 7) (1932) 537.
[26] R.S. Patil, V.R. Shaikh, P.D. Patil, A.U. Borse, K.J. Patil, J. Mol. Liq. 200 (2014) 416.
[27] N. Martinus, C.D. Sinclair, C.A. Vincent, Electrochim. Acta 22 (1977) 1183.
[28] J.E. Desnoyers, G. Perron, J. Solut. Chem. 1 (1972) 199.
[29] D.S. Viswanath, T. Ghosh, D.H.L. Prasad, N.V.K. Dutt, K.Y. Rani, Viscosity of Liquids, Springer, Berlin, 2007407–442.
[30] A.A. Zavitsas, Chem. Eur. J. 16 (2010) 5942.
[31] Y. Marcus, Ions in Solution and Their Solvation, John Wiley & Sons, Inc., Hoboken, New Jersey, 2015.
[32] A.G. Lyapin, E.L. Gromnitskaya, I.V. Danilov, V.V. Brazhkin, RSC Adv. 7 (2017) 33278.
[33] J. Geschwind, H. Frey, Macromolecules 46 (2013) 3280.
[34] V. Calvino-Casilda, G. Mul, J.F. Fernandez, F. Rubio-Marcos, M.A. Banares, Appl. Catal., A 409–410 (2011) 106.
[35] J.S. Choi, F.S. Hubertson Simanjuntaka, J. Young Oh, K.I. Lee, S.D. Lee, M. Cheong, H.S. Kim, H. Lee, J. Catal. 297 (2013) 248.
[36] M.S. Ding, J. Chem. Eng. Data 49 (2004) 1469.
[37] K. Izutsu, Electrochemistry in Nonaqueous Solutions, Wiley-VCH, Weinheim, 2002206–207.
[38] J.R. MacCallum, A.S. Tomlin, C.A. Vincent, Eur. Polym. J. 22 (1986) 787.
[39] L. Niedzicki, M. Kasprzyk, K. Kuziak, G.Z. Zukowska, M. Marcinek, W. Wieczorek, M. Armand, J. Power Sources 196 (2011) 1386.
[40] J. Barthel, Angew. Chem. Int. Ed. Eng. 7 (1968) 260.
[41] L. Niedzicki, M. Kasprzyk, K. Kuziak, G.Z. Zukowska, M. Armand, M. Bukowska, M. Marcinek, P. Szczecinski, W. Wieczorek, J. Power Sources 192 (2009) 612.
[42] R. Haase, Angew. Chem. Int. Ed. Eng. 4 (1965) 485.
[43] J. Cazes, Encyclopedia of Chromatography, CRC Press, Boca Raton, 2001273.
[44] S. Boileau, P. Hemery, Electrochim. Acta 21 (1976) 647.
[45] J. Clark, Chem. Rev. 80 (1980) 429–452.
[46] I.N. Rozhkov, I.L. Knunyant, Dokl. Akad. Nauk SSSR 199 (1971) 614.